Low-Threshold 795 nm Oxide-Confined Distributed Feedback Lasers With Surface Gratings

Pingping Qiu, Hengjie Zhou, Tongxin Wang, Qiuhua Wang, and Qiang Kan

***Abstract*—795 nm oxide-confined distributed feedback (DFB) lasers have been developed. The oxide-confined structure is used to realize lateral optical and current confinement, and the first-order surface gratings offer the frequency selectivity for single-longitudinal mode operation. The fabricated 200-μm-long devices exhibited a low-threshold current of ∼4.8 mA, a 3-dB modulation bandwidth of ∼5.8 GHz and maintained stable single mode operation around 795 nm with side mode suppression ratio (SMSR) as high as ∼40 dB. The simple and compact laser structure greatly reduces the difficulty of device design and fabrication compared with traditional DFB lasers. The characteristics of the laser, including low-threshold current, single mode stability and potentially narrow spectral linewidth, make it a suitable candidate for applications in absorption spectroscopy of the rubidium D1 line, chip-scale atomic clocks, magnetometers, and gyroscopes.**

***Index Terms*—Distributed feedback laser, surface grating, single mode, low threshold current.**

I. Introduction

SIMPLE, robust, and single-mode lasers emitting in the wavelength of ∼795 nm are of great interest for applications in absorption spectroscopy of the rubidium D1 line, chip-scale atomic clocks, magnetometers, and gyroscopes [1], [2], [3]. These applications typically require a laser source of stable single-mode operation with narrow spectral linewidth and the possibility of fine tuning of the wavelength. Distributed feedback (DFB) lasers have proved to be convenient single-mode laser sources owing to their excellent spectral purity, low power consumption, structure compactness and easy integration [4], [5], [6]. However, conventional DFB lasers with buried gratings require two or more epitaxial growth steps. The re-growth complicates the device fabrication and increases the device cost. Particularly it brings challenges to the device performance, yield and reliability when Al-contained materials are used [7], [8].

The use of surface gratings avoids the problematic epitaxial re-growth and simplifies the fabrication process, with modest impacts on device performance. Previous reports have demonstrated that surface grating DFB lasers have extraordinary operating performances, such as high power, high side-mode suppression ratio (SMSR), and narrow spectral linewidth [9], [10], [11]. Generally, there are two methods to realize DFB lasers with surface grating, namely laterally coupled surface gratings and vertically coupled surface gratings [12], [13], [14]. The laterally-coupled gratings are placed along the sidewalls of the ridge waveguides, which works only for lasers with a narrow ridge due to the weak coupling of the fundamental lateral mode with the grating. Recently, a narrow linewidth 790 nm laterally coupled surface grating laser was reported [15]. An average linewidth of 207 kHz was obtained for a 1500-μm-long device with 5th order surface gratings. However, deeply etched grating and waveguide were implemented to ensure minimal losses for the Bragg mode, which posed stringent fabrication control. The vertically-coupled gratings are etched within ridge waveguides, which allows a better overlap of the mode with the grating. However, optical waveguide mode must be carefully designed to reduce the absorption loss caused by the metal contacts on the top of grating, or a lateral-current-injection method is required [16], [17]. Zhang et al. demonstrated an 850 nm two-section surface grating DFB laser composed of a 150-μm gain section and a 100-μm reflection section with a low threshold current of 8 mA [16]. The top contact metals are placed on two side ridges thus avoiding unwanted optical absorption from the electrodes. Precise fabrication control is required for such a sophisticated device structure.

In this letter, we present the design and fabrication of a low-threshold current, single mode 795 nm oxide-confined DFB laser with surface gratings. Single lateral mode operation has been achieved for a 45-μm-wide ridge waveguide by introducing an oxide-confined structure, which greatly reduces the complexity of device design and fabrication. The first-order surface gratings offering frequency selectivity for single longitudinal mode operation have been optimized to realize low threshold currents and the targeted emission wavelength of 795 nm. The 200-μm-long fabricated laser exhibits a low threshold current of ∼4.8 mA, a 3-dB modulation bandwidth of ∼5.8 GHz and stable single mode operation around 795 nm with a SMSR of ∼40 dB.

Manuscript received 24 July 2023; revised 4 September 2023; accepted 22 September 2023. Date of publication 26 September 2023; date of current version 19 October 2023. This work was supported by the National Natural Science Foundation of China under Grants 62134008 and 62204237. *(Corresponding author: Qiang Kan.)*

Pingping Qiu, Hengjie Zhou, and Qiuhua Wang are with the Key Laboratory of Semiconductor Materials Science, Institute of Semiconductors, Chinese Academy of Sciences, Beijing 100083, China (e-mail: ppqiu@semi.ac.cn; hjzhou@semi.ac.cn; qhwang@semi.ac.cn).

Tongxin Wang and Qiang Kan are with the Key Laboratory of Semiconductor Materials Science, Institute of Semiconductors, Chinese Academy of Sciences, Beijing 100083, China, and also with the Center of Materials Science and Optoelectronics Engineering, University of Chinese Academy of Sciences, Beijing 100049, China (e-mail: wangtx@semi.ac.cn; kanqiang@semi.ac.cn).

Digital Object Identifier 10.1109/JPHOT.2023.3319314

© 2023 The Authors. This work is licensed under a Creative Commons Attribution 4.0 License. For more information, see https://creativecommons.org/licenses/by/4.0/

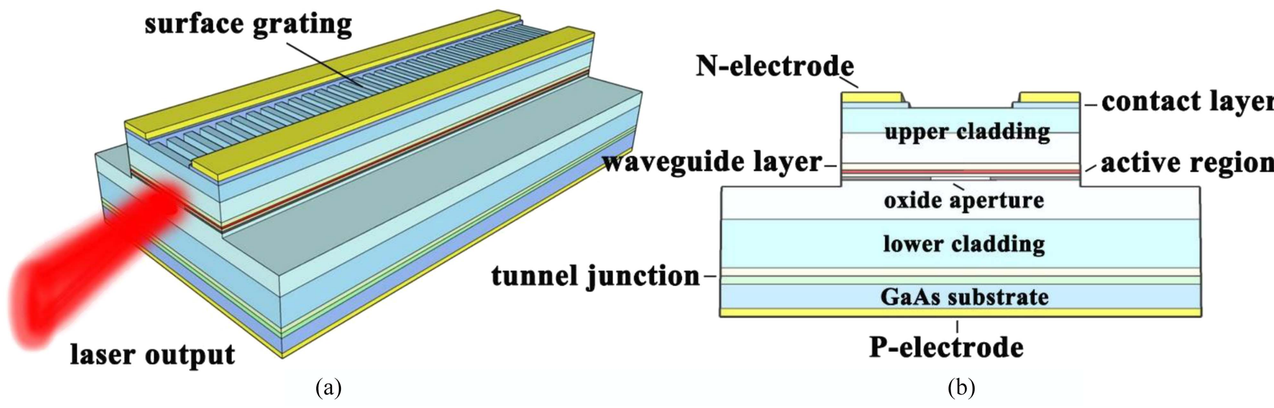

Fig. 1. Schematic structures of the device: (a) 3-dimensional view, (b) cross section of the laser structure.

TABLE I
795 NM OXIDE-CONFINED DFB LASER EPITAXIAL STRUCTURE

Layer	Material	Thickness/nm	Doping/cm^{-3}
1	GaAs	150	5x10^{18}
2	$Al_{0.32}Ga_{0.68}As$	250	1x10^{18}
3	$Al_{0.3}Ga_{0.7}As$	50	5x10^{17}
4	$Al_{0.3}Ga_{0.7}As$	40	undoped
5	$Al_{0.07}Ga_{0.93}As$	6	undoped
6	$Al_{0.35}Ga_{0.65}As$	6	undoped
7	$Al_{0.07}Ga_{0.93}As$	6	undoped
8	$Al_{0.35}Ga_{0.65}As$	6	undoped
9	$Al_{0.07}Ga_{0.93}As$	6	undoped
10	$Al_{0.3}Ga_{0.7}As$	40	undoped
11	$Al_{0.65}Ga_{0.35}As$	40	5x10^{17}
12	$Al_{0.98}Ga_{0.02}As$	20	1x10^{18}
13	$Al_{0.65}Ga_{0.35}As$	1500	1x10^{18}
14	GaAs	15	1x10^{20}
15	GaAs	15	5x10^{19}
16	GaAs	500	3x10^{18}

II. Device Structure and Fabrication

Fig. 1 presents the structure of the device, whilst Table I presents the layer structure. The epilayer structure, grown on a n-doped GaAs substrate by metal organic chemical vapor deposition (MOCVD), comprises three undoped $Al_{0.07}Ga_{0.93}As/Al_{0.35}Ga_{0.65}As$ quantum wells active region, placed between 80 nm thick undoped $Al_{0.3}Ga_{0.7}As$ waveguide layers. The 20 nm Al-rich oxide layer embedded in the lower p-doped $Al_{0.65}Ga_{0.35}As$ cladding layer was oxidized to form the oxide aperture for lateral optical and current confinement. In order to make all the layers still epitaxially growable on a traditional n-doped GaAs substrate, a p++/n++ GaAs tunneling junction was employed. It should be noted that the N-i-P structure also favors current spreading and reduction of absorption loss since the limited upper cladding thickness and large optical field overlapping with the upper cladding. Above the upper cladding, 150 nm highly n-doped GaAs contact layer was grown. The surface gratings were located in the surface of the ridge waveguide where the GaAs contact layer was selectively etched to reduce optical absorption.

In a conventional ridge waveguide laser, lateral mode confinement is offered by a narrow ridge waveguide structure. In our device, a wide ridge is adopted for the sake of current injection, and an oxide-confined structure is further implemented to realize lateral mode and current confinement thus a low threshold single mode device. Fig. 2(a) shows the simulated mode distribution of the fundamental mode for the oxide aperture with the width of 2 μm, where we can see that the mode field is mainly distributed in the center of the ridge due to the oxide-confined structure. The lateral mode size and mode number are determined by the width of the oxide aperture, thus single mode operation can be maintained even at a wide ridge waveguide. Furthermore, the device structure is carefully designed to enhance the optical field intensity in the upper cladding layer while still maintaining sufficient optical confinement in the active region. Larger optical field in the upper cladding layer provides a high coupling coefficient with a shallow etched surface grating. Fig. 2(b) presents the calculated coupling coefficient and optical confinement factor of the active region versus the etching depth of the grating. The grating coupling coefficient defined as $K = (2 * \Delta n_{eff})/\lambda_{Bragg}$ is up to 335 cm^{-1} with a 50 nm shallowly etched surface grating, where Δn_{eff} is the effective index difference of the fundamental mode in the ridge waveguide with/without the surface grating [18], [19]. And, the optical confinement factor of the active region maintained between 4.9%~6.1% with varied etching depth of the grating. More exact information in terms of reflectivity bandwidth and group velocity can be obtained with an equivalent surface current method [20]. In order to have a precise control of the laser emission wavelength, the grating periods defined as $\wedge_g = (\lambda_{Bragg} * m)/(2 * n_{eff})$ are estimated with the grating etching depth varied from 50 nm to 150 nm. As shown in Fig. 2(c), in order to achieve an emission wavelength of 795 nm, the grating periods are increased from 118.7 nm to 119.5 nm as the grating etching depth increases from 50 nm to 150 nm. This is mainly because the reduced effective index of the mode in the waveguide as the grating etching depth deepens.

The surface gratings offer the frequency selectivity for single-longitudinal mode operation. Fig. 3(a) displays the simulated transmission spectra of the uniform surface grating and λ/4 phase shifted grating. As shown in Fig. 3(b), a quarter wavelength low index is introduced into the uniform grating to form the

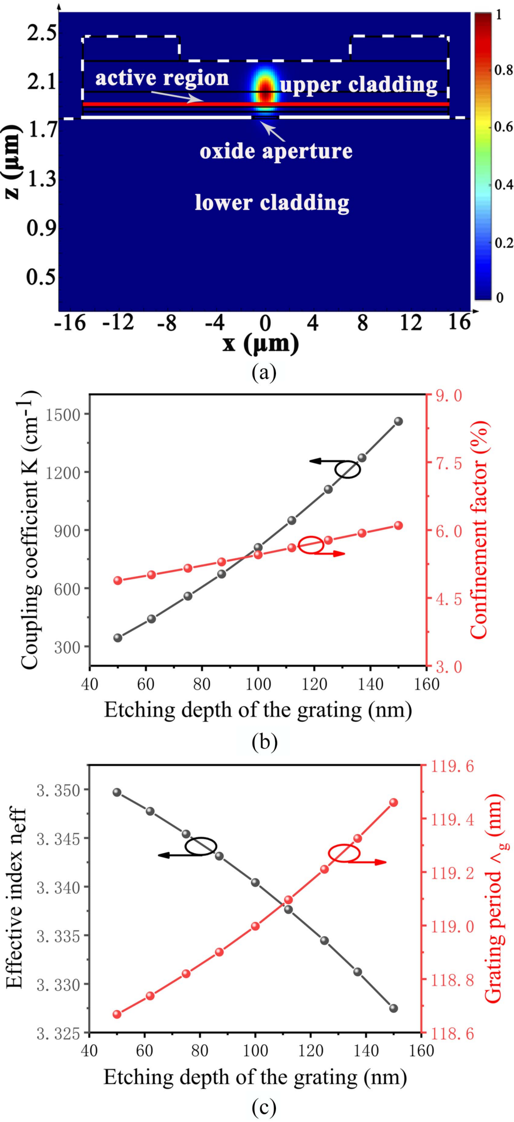

Fig. 2. (a) Simulated mode distribution of the fundamental mode in the ridge waveguide. (b) Calculated coupling coefficient K and confinement factor versus the etching depth of the grating. (c) Calculated effective index and grating period versus the etching depth of the grating.

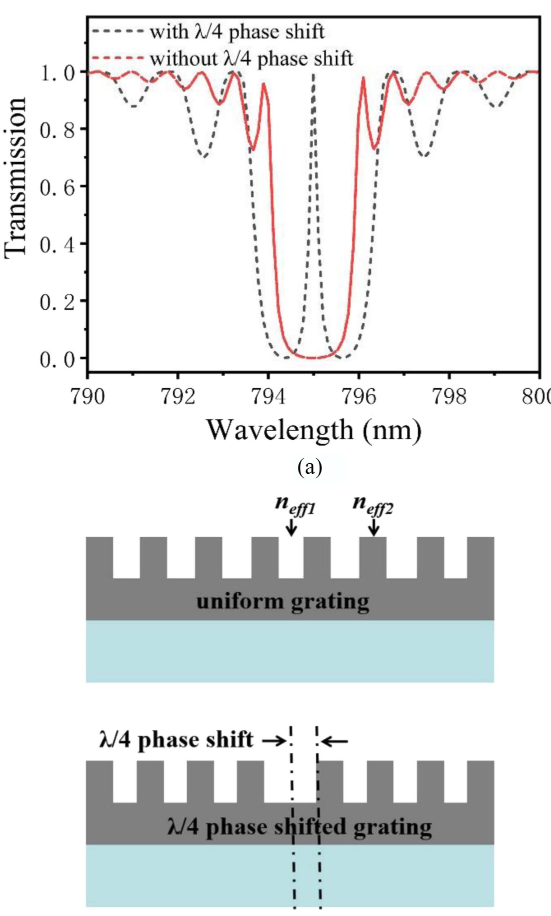

Fig. 3. (a) Simulated transmission spectra of the uniform grating and λ/4 phase shifted grating. (b) Schematics of uniform surface grating and λ/4 phase shifted grating.

λ/4 phase shifted grating. Theoretically, two modes equally spaced on each side of the Bragg wavelength reach threshold simultaneously (red line in Fig. 3(a)). In practice, additional perturbations such as reflections from uncoated cleaves at the end will break the degeneracy. However, a yield problem still exists due to the random relative phase of reflection from the cleave [18]. Therefore, to achieve a high single mode yield, λ/4 phase shifted grating is preferable. The inserted λ/4 low index brings an additional $\pi/2$ phase change, which leads to the lasing of the Bragg wavelength (black line in Fig. 3(a)). In the simulation, n_{eff1} and n_{eff2} are obtained by calculating the effective index of the fundamental mode in the ridge waveguide with/without the surface grating, which corresponds to 3.338 and 3.357 for the grating etching depth of 60 nm.

The device has been fabricated by a process similar to the process described in reference [21]. First, the top GaAs layer is selectively wet etched by using citric acid/H_2O_2. The ridge waveguide is formed by inductively coupled plasma reaction ion etching (ICP-RIE) down to the active region to expose the oxide layer using $BCl_3/Ar/Cl_2$, with photoresist as the mask. Afterwards, a narrow rectangle oxide aperture for lateral optical and current confinement is formed by selectively wet oxidization of a 20 nm-thick $Al_{0.98}Ga_{0.02}As$ layer at 400 °C. An in situ near-infrared microscope image of a 2-μm-wide rectangle oxide aperture for the ridge waveguide width of 45 μm is presented in Fig. 4(a). Then, 300-nm Si_3N_4 is deposited for electrical isolation, and the AuGeNi/Au-N electrode is patterned by magnetron sputtering after opening the contact window. To define the surface grating, a mask pattern is formed by ZEP520A electron beam resist which directly served as the etching mask for the etching of AlGaAs grating. Fig. 4(b) shows the scanning electron microscopic (SEM) image of the fabricated surface grating with grating period of ∼119 nm. Finally, the epi-wafer is thinned to ∼100 μm, and the bottom ohmic (Au/Ge/Ni/Au) contacts formed and annealed using rapid thermal annealing at 350 °C for 35 s. The fabricated wafer is cleaved into single chips of 200 μm cavity length. Fig. 4(c) presents the microscope images of the fabricated wafer and a cleaved single chip integrated on a copper heat sink for testing.

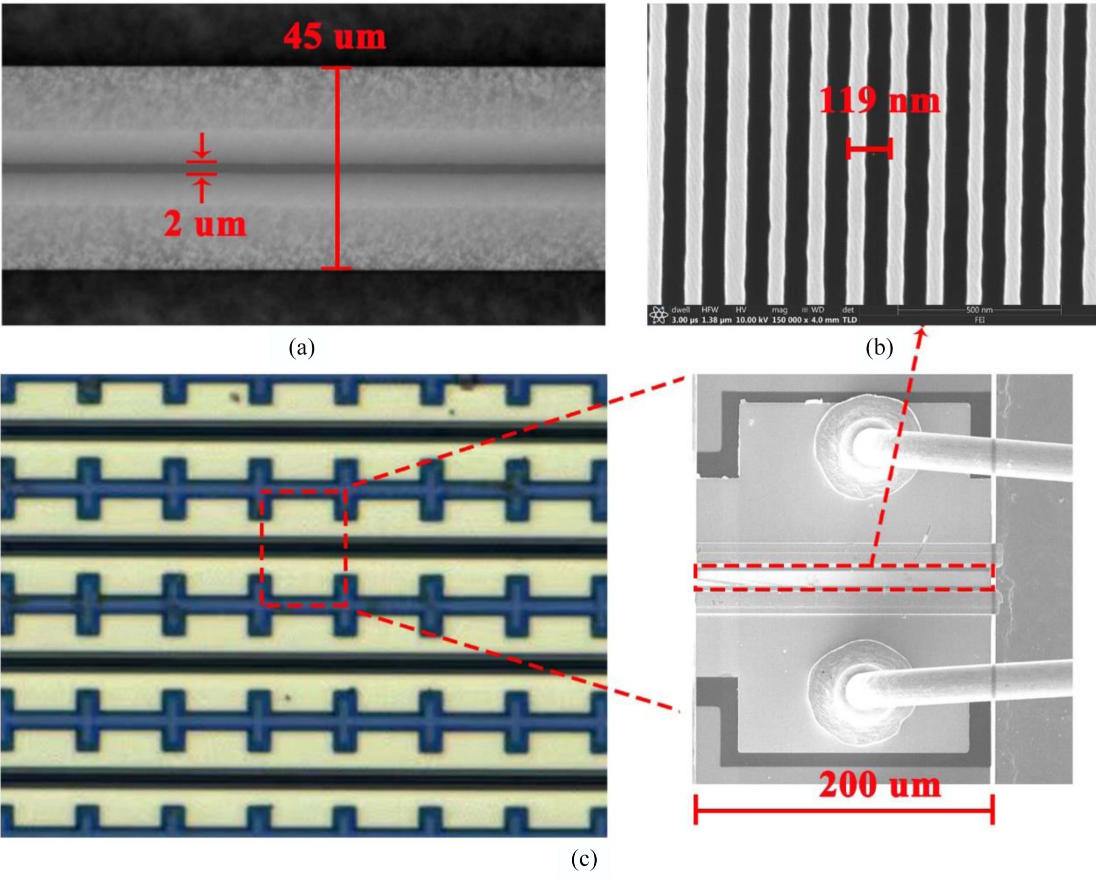

Fig. 4. (a) In situ near infrared microscope image of the rectangle oxide aperture with aperture width of 2 μm for the ridge waveguide width of 45 μm. (b) SEM of the surface grating with grating period of 119 nm. (c) The microscope images of the fabricated wafers and a cleaved single chip integrated on a copper heat sink.

III. Results and Discussions

Fabricated wafers are cleaved into single chips of 200 μm cavity length and integrated on a copper heat sink with the thermoelectric cooler (TEC) to control the devices' temperature. Fig. 5(a) shows the measured light–current–voltage (L-I-V) curve of the device at a temperature of 25 °C. The laser has a threshold current of $\sim$13 mA and a maximum output power of 3.3 mW at a bias current of 42 mA under continuous wave (CW) operation. The differential resistance and slope efficiency of the device are estimated to be about 26 Ω and 0.15 mW/mA respectively. In order to realize a laser emission wavelength of 795 nm, surface gratings with different periods are prepared. As shown in Fig. 5(b), the lasing wavelength varied from 784.6 nm to 800.3 nm as the grating periods increased from 117 nm to 120 nm. A lasing wavelength of 795.1 nm is achieved at the grating period of 119 nm with an injection current of 35 mA. Fig. 5(c) and (d) present the emission wavelength of the same device versus bias current and heat-sink temperature respectively. The lasing wavelength increased from 794.144 nm to 795.432 nm as the bias current increased from 15 mA to 35 mA at a heat-sink temperature of 25 °C. A wavelength–current tuning coefficient of $\sim$0.064 nm/mA is estimated. Also, the lasing wavelength increased from 794.1 nm to 796.264 nm as the heat-sink temperature increased from 10° to 40° at a bias current of 35 mA. A wavelength–temperature tuning coefficient of $\sim$0.072 nm/° is estimated. The device maintains stable single-mode operation with SMSR > 35 dB, throughout all bias currents and heat-sink temperature.

To extract the coupling coefficient of the surface grating, the near-threshold spectrum of the device is measured. As shown in Fig. 6(a), a stopband of $\sim$1.31 nm is obtained for a 200 μm long device with uniform gratings. The grating coupling coefficient K then can be estimated from $\Delta\lambda_s$ using the following formula [22], [23].

$$\Delta\lambda_s = \frac{\left(\lambda_{Bragg}^2\right)}{\pi n_g}\sqrt{\left((\pi/\mathrm{L})^2 + \mathrm{K}^2\right)},$$

where λ_{Bragg} is the Bragg wavelength of the grating, L denotes the cavity length, and n_g is group index of the waveguide defined as $n_g = n_{eff} - \lambda((\mathrm{d}n_{eff})/\mathrm{d}\lambda)$. By calculating the effective index of fundamental mode in the waveguide versus wavelength (shown in Fig. 6(b)), a group index of 3.48 is obtained. Therefore, the coupling coefficient of the fabricated grating is estimated to be about 164 cm^{-1}. The extracted value is much lower than expected, which can be attributed to the imperfect etching profile with the tilt and rough side walls and inappropriate duty cycle of the fabricated grating as shown in the inset of Fig. 6(b). The surface grating profile is optimized to enhance the coupling coefficient in the following work.

Fig. 5. (a) L-I-V curve of the fabricated device. (b) Spectra of the fabricated devices with grating periods of 117 nm, 118 nm, 119 nm and 120 nm. (c) Emission wavelength of the same device versus bias current, the wavelength–current coefficient is 0.064 nm/mA. (d) Emission wavelength of the same device versus heat-sink temperature, the wavelength–temperature coefficient is 0.072 nm/°.

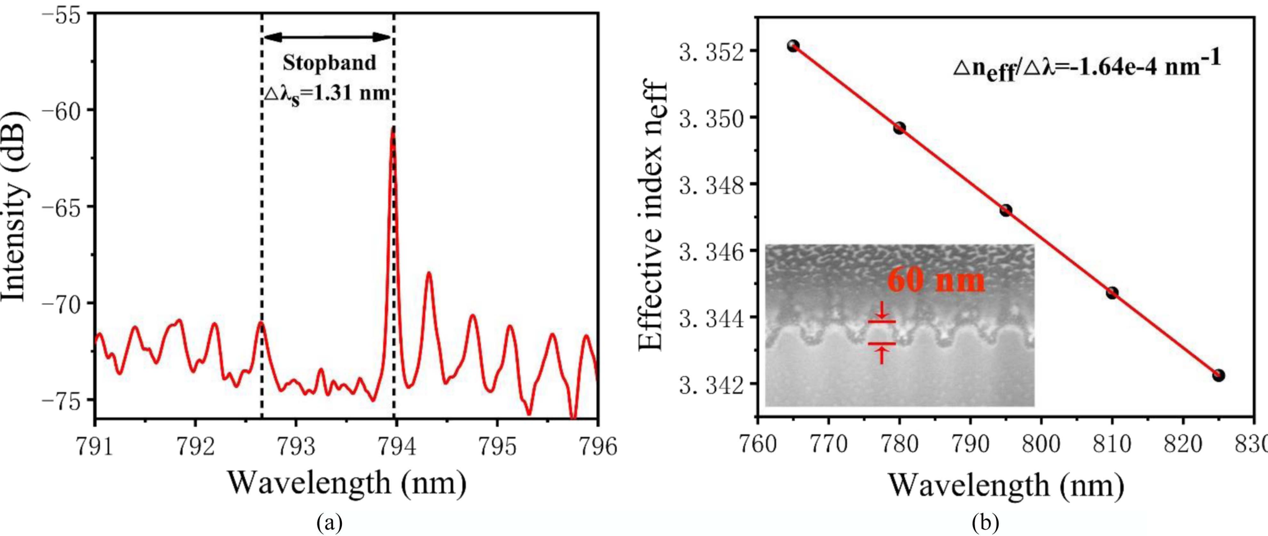

Fig. 6. (a) Measured near-threshold spectrum of the device. (b) Calculated effective index of fundamental mode in the waveguide versus wavelength with $\Delta n_{eff}/\Delta\lambda = -1.64\text{e-}4\ \text{nm}^{-1}$ (inset: SEM image of the fabricated surface gratings with etching depth of ∼60 nm).

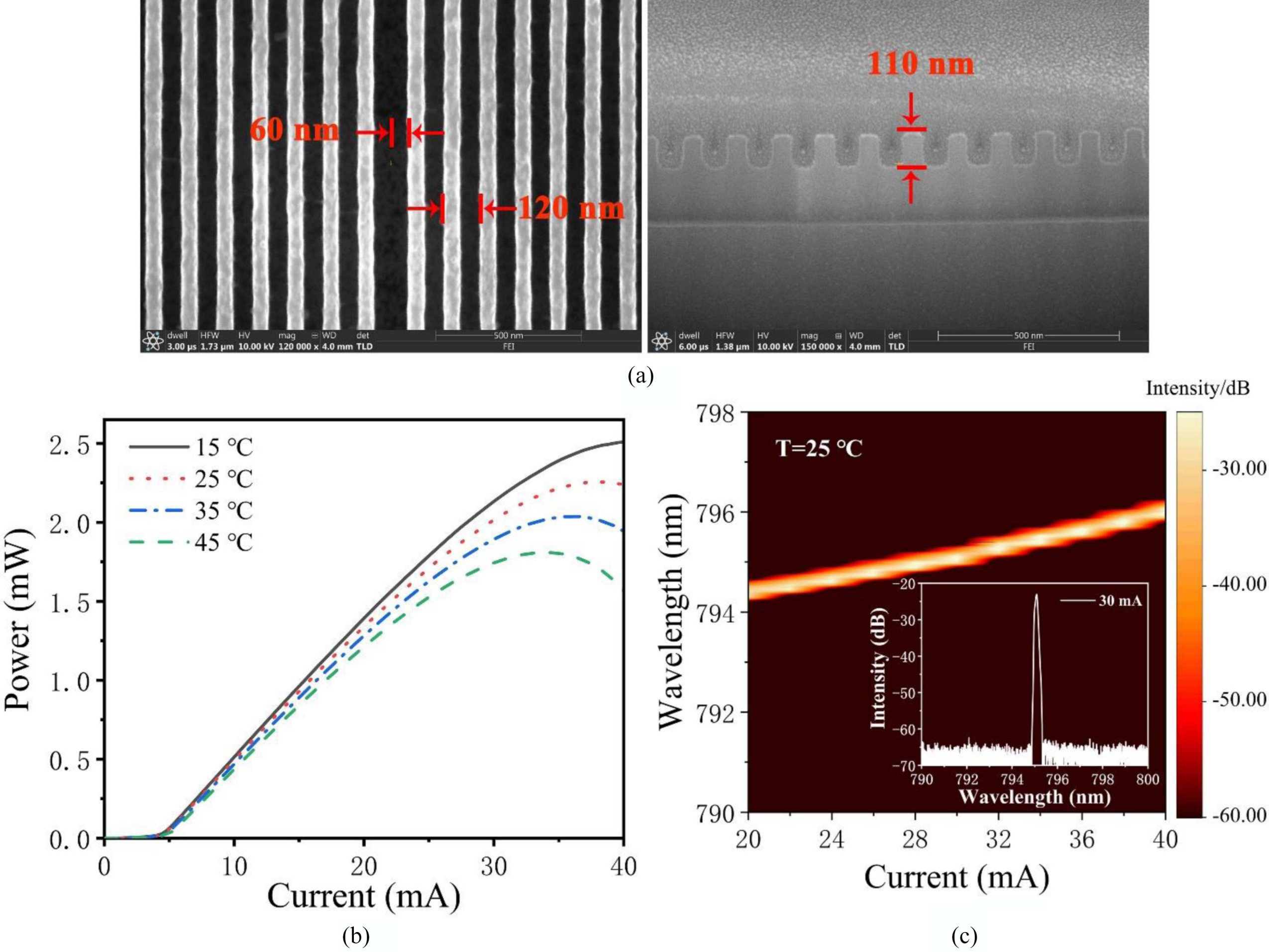

Fig. 7. (a) SEM images of the prepared λ/4 phase shifted surface gratings. (b) Temperature-dependent L-I curves of the optimized device. (c) Map of optical spectra for different currents (inset: Optical spectrum at 30 mA).

The grating coupling coefficient is much lower than expected. The decreased coupling coefficient leads to an increased threshold of the laser. Therefore, we optimized the surface gratings and a quarter wavelength low index (∼60 nm) is introduced into the uniform grating to form the λ/4 phase shifted grating. The SEM images of the prepared λ/4 phase shifted surface gratings are presented in Fig. 7(a). The optimized surface gratings have a grating period of ∼120 nm and an enhanced etching depth of ∼110 nm exhibiting a much better profile such as relatively vertical side walls and moderate duty cycle. As can be seen from the measured temperature-dependent L-I curves in Fig. 7(b), the threshold current reduced to ∼4.8 mA and an output power of ∼2.2 mW is achieved at 25 °C under CW operation for the optimized device. The corresponding threshold current density is as low as ∼1.2 kA/cm^2. By decreasing the heat-sink temperature to 15 °C, a maximum output power of ∼2.5 mW can be obtained due to the relieved heating effect. The improved grating profile and etching depth result in an enhanced coupling coefficient thus a decreased threshold current of the device. Fig. 7(c) presents the map of optical spectra of the device with bias currents range from 20 mA to 40 mA at 25 °C, where we can observe that the laser maintains stable single mode operation without any mode hopping within the current range. From the wavelength shift of 1.63 nm between 20 mA and 40 mA, a wavelength-current tuning coefficient of ∼0.082 nm/mA is estimated. The inset in Fig. 7(c) shows the spectrum at a current of 30 mA corresponding to a power of ∼1.5 mW. A lasing wavelength of 795 nm and a SMSR of ∼40 dB can be extracted. The single-mode lasing wavelength of 795 nm and the possibility of its fine tuning by modifying the bias current and operation temperature demonstrate great potential of using the fabricated lasers in ^{87}Rb-based miniaturized atomic clocks, magnetometers, and gyroscopes.

Single mode laser source for ^{87}Rb-based atomic clocks must be modulated at 3.4 GHz thus a modulation bandwidth of >3.4 GHz is required [24]. Fig. 8(a) presents the small-signal modulation response of the fabricated device. A sufficient 3-dB bandwidth of ∼5.8 GHz is obtained at a bias current of 30 mA. Furthermore, far-field divergence angles are measured to characterize the beam property of the device. As can be seen from Fig. 8(b), a typical single-mode far-field pattern is achieved with the full width at half maximum (FWHM) divergence angle of 17° × 43° in the lateral and vertical direction, respectively, at room temperature and a bias current of 30 mA.

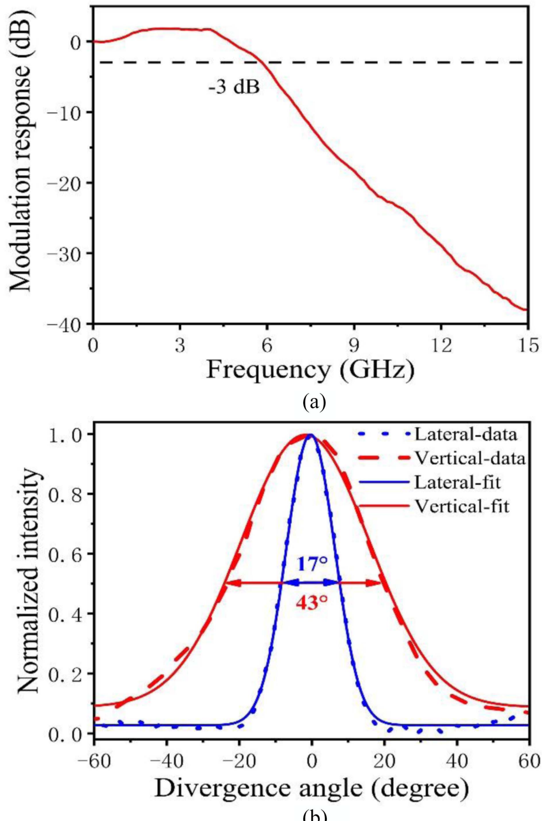

Fig. 8. (a) Small-signal modulation response curve of the 795 nm oxide-confined DFB laser with surface gratings at 25 °C and a bias current of 30 mA. (b) Far-field divergence angle of the device.

IV. Conclusion

In conclusion, we have designed and experimentally demonstrated a 795 nm low-threshold current surface grating DFB laser with an oxide-confined structure. By using a 2-μm-wide oxide aperture and a first-order surface grating, stable single mode operation without any mode hopping has been realized for a 45-μm-wide ridge waveguide. The prepared 200-μm-long device exhibiting a low threshold current of $\sim$4.8 mA and a sufficient 3-dB modulation bandwidth of $\sim$5.8 GHz has a lasing wavelength of $\sim$795 nm with SMSR as high as $\sim$40 dB at the bias current of 30 mA. Adoption of such laser structures greatly reduces the difficulty of device design and fabrication compared with traditional DFB lasers. The simple manufacturing process and stable performance give this low-threshold laser broad application prospects in the fields of absorption spectroscopy of the rubidium D1 line and atomic clocks, magnetometers, gyroscopes.

References

[1] Y. Zhou et al., "Large-aperture single-mode 795 nm VCSEL for chip-scale nuclear magnetic resonance gyroscope with an output power of 4.1 mW at 80°," *Opt. Exp.*, vol. 30, no. 6, pp. 8991–8999, Mar. 2022, doi: 10.1364/OE.450118.

[2] A. Klehr et al., "High power DFB lasers for D1 and D2 caesium absorption spectroscopy and atomic clocks," *Proc. SPIE*, vol. 7230, 2008, Art. no. 69091E, doi: 10.1117/12.761092.

[3] I. A. Derebezov, V. A. Haisler, A. K. Bakarov, A. K. Kalagin, A. I. Toropov, and M. M. Kachanova, "Single-mode vertical-cavity surface emitting lasers for ^{87}Rb-based chip-scale atomic clock," *Semiconductors*, vol. 44, no. 11, pp. 1422–1426, Nov. 2010, doi: 10.1134/S1063782610110084.

[4] M. Xiang et al., "Wide-waveguide high-power low-RIN single-mode distributed feedback laser diodes for optical communication," *Opt. Exp.*, vol. 30, no. 17, pp. 30187–30197, Aug. 2022, doi: 10.1364/OE.464598.

[5] A. Klehr et al., "High-power 894 nm monolithic distributed-feedback laser," *Opt. Exp.*, vol. 15, no. 18, pp. 11364–11369, Sep. 2007, doi: 10.1364/OE.15.011364.

[6] X. Sun et al., "Regrowth-free AlGaInAs MQW polarization controller integrated with a sidewall grating DFB laser," *Photon. Res.*, vol. 11, no. 4, pp. 622–630, Apr. 2023, doi: 10.1364/PRJ.480676.

[7] F.-J. Vermersch et al., "High-power narrow linewidth distributed feedback lasers with an aluminium-free active region emitting at 852 nm," *IEEE Photon. Technol. Lett.*, vol. 20, no. 13, pp. 1145–1147, Jul. 2008, doi: 10.1109/LPT.2008.924903.

[8] N. Von Bandel et al., "Al-free active region laser diodes at 894 nm for compact Cesium atomic clocks," *Proc. SPIE*, vol. 9382, 2015, Art. no. 93820L, doi: 10.1117/12.2076750.

[9] E. Di Gaetano, S. Watson, E. McBrearty, M. Sorel, and D. J. Paul, "Sub-megahertz linewidth 780.24 nm distributed feedback laser for ^{87}Rb applications," *Opt. Lett.*, vol. 45, no. 13, pp. 3529–3532, Jul. 2020, doi: 10.1364/OL.394185.

[10] H. Virtanen, T. Uusitalo, M. Karjalainen, S. Ranta, J. Viheriälä, and M. Dumitrescu, "Narrow-linewidth 780-nm DFB lasers fabricated using nanoimprint lithography," *IEEE Photon. Technol. Lett.*, vol. 30, no. 1, pp. 51–54, Jan. 2018, doi: 10.1109/LPT.2017.2772337.

[11] K. Tian et al., "High-power distributed feedback lasers with high-order surface curved gratings," *Opt. Lett.*, vol. 47, no. 21, pp. 5626–5629, Nov. 2022, doi: 10.1364/OL.472345.

[12] J. H. Kang et al., "Continuous-wave operation of DFB laser diodes based on GaN using 10th-order laterally coupled surface gratings," *Opt. Lett.*, vol. 45, no. 4, pp. 935–938, Feb. 2020, doi: 10.1364/OL.385002.

[13] H. Wenzel, J. Fricke, J. Decker, P. Crump, and G. Erbert, "High-power distributed feedback lasers with surface gratings: Theory and experiment," *IEEE J. Sel. Topics Quantum Electron.*, vol. 21, no. 6, Nov./Dec. 2015, Art. no. 1502707, doi: 10.1109/JSTQE.2015.2429892.

[14] T. Shindo et al., "Lateral-current-injection type membrane DFB laser with surface grating," *IEEE Photon. Technol. Lett.*, vol. 25, no. 13, pp. 1282–1285, Jul. 2013, doi: 10.1109/LPT.2013.2261980.

[15] B. Janjua, M. L. Iu, Z. Yan, P. Charles, E. Chen, and A. S. Helmy, "Distributed feedback lasers using surface gratings in Bragg waveguides," *Opt. Lett.*, vol. 46, no. 15, pp. 3689–3692, Aug. 2021, doi: 10.1364/OL.431292.

[16] P. Zhang et al., "850 nm GaAs/AlGaAs DFB lasers with shallow surface gratings and oxide aperture," *Opt. Exp.*, vol. 27, no. 22, pp. 31225–31234, Oct. 2019, doi: 10.1364/OE.27.031225.

[17] T. Shindo et al., "Lateral-current-injection distributed feedback laser with surface grating structure," *IEEE J. Sel. Topics Quantum Electron.*, vol. 17, no. 5, pp. 1175–1182, Sep./Oct. 2011, doi: 10.1109/JSTQE.2011.2131636.

[18] L. A. Coldren, S. W. Corzine, and M. L. Mashanovitch, *Diode Lasers and Photonic Integrated Circuits*, 2nd ed. Hoboken, NJ, USA: Wiley, 2012.

[19] H. Tan et al., "Analysis of first-order gratings in silicon photonic waveguides," *IEEE Photon. J.*, vol. 14, no. 6, Dec. 2022, Art. no. 6659110, doi: 10.1109/JPHOT.2022.3211456.

[20] J. Huang, K. Liu, J. K. Butler, N.-H. Sun, and G. A. Evans, "First-order grating coupling coefficients in asymmetric three-layer waveguides for transverse electric modes," *J. Lightw. Technol.*, vol. 35, no. 11, pp. 2200–2210, Jun. 2017, doi: 10.1109/JLT.2017.2661842.

[21] P. Qiu, B. Wu, P. Fu, M. Li, Y. Xie, and Q. Kan, "Fabrication and characterization of low-threshold single fundamental mode VCSELs with dielectric DBR mirror," *IEEE Photon. J.*, vol. 13, no. 4, Aug. 2021, Art. no. 1500106, doi: 10.1109/JPHOT.2021.3089710.

[22] N. Matuschek, F. X. Kartner, and U. Keller, "Exact coupled-mode theories for multilayer interference coatings with arbitrary strong index modulations," *IEEE J. Quantum Electron.*, vol. 33, no. 3, pp. 295–302, Mar. 1997, doi: 10.1109/3.555995.

[23] M. Razeghi et al., "Low-threshold distributed feedback lasers fabricated on material grown completely by LP-MOCVD," *IEEE J. Quantum Electron.*, vol. 21, no. 6, pp. 507–511, Jun. 1985, doi: 10.1109/JQE.1985.1072707.

[24] C. M. Long and K. D. Choquette, "Optical characterization of a vertical cavity surface emitting laser for a coherent population trapping frequency reference," *J. Appl. Phys.*, vol. 103, no. 3, Feb. 2008, Art. no. 033101, doi: 10.1063/1.2838175.